AIAA Aviation Forum and ASCEND co-located Conference Proceedings
29 July - 2 August 2024, Las Vegas, Nevada
AIAA AVIATION FORUM AND ASCEND 2024
10.2514/6.2024-3990

Advanced Propulsion System Evaluation for Real-World Short-Haul Operations: Open Rotor vs. UHBPR Turbofan

Conor Gallagher[1], Charles Stuart[2], Stephen Spence[3]
Trinity College Dublin, the University of Dublin, Ireland

This study aims to evaluate the real-world benefits of two advanced propulsion system concepts through enhanced coupling of aircraft conceptual design and flight operations. Baseline aircraft models of the B737-NG and B737-MAX aircraft were developed using a combination of SUAVE and NPSS, and were subsequently validated and calibrated against real-world flight data using a novel real-world operations model. The baseline aircraft models yielded exceptional accuracy over a wide range of flights, yielding average total fuel burn errors between 1.5-1.0% for the B737-NG and B737-MAX aircraft, respectively. Numerical NPSS models of the UHBPR turbofan and CROR engine were developed and validated against numerical models in published literature, which were then integrated with the calibrated B737-MAX airframe model to develop the advanced aircraft configurations. The baseline B737-MAX, along with both advanced aircraft configurations were simulated over a full day of flight operations to and from Irish airports, where the fuel burn performance of each configuration was evaluated in a comparative analysis. Results show that the UHBPR and CROR propulsion systems could result in fuel burn reductions of 14.0% and 23.3%, respectively, when compared to the baseline B737-MAX aircraft. Furthermore, significantly increased performance benefits were observed for the CROR engine for mission ranges below 500 NM, increasing the impact of this configuration for short-haul and regional airlines.

I. Nomenclature

ADS-B	Automatic Dependent Surveillance-Broadcast	QAR	Quick-Access Recorder
ATAG	Air Transport Action Group	RTO	Rolling Take-Off
BPR	Bypass Ratio	SAF	Sustainable Aviation Fuel
CO2	Carbon Dioxide	SLS	Sea-Level Static
CRZ	Cruise	SUAVE	Stanford University Aerospace Vehicle Environment
CROR	Contra-Rotating Open-Rotor	TOC	Top-Of-Climb
GS	Ground Speed	TOW	Take-Off Weight
ICAO	International Civil Aviation Organisation	TSFC	Thrust Specific Fuel Consumption
L/D	Lift-to-Drag Ratio	UDF	Un-Ducted Fan
MTOW	Maximum Take-Off Weight	UHBPR	Ultra-High Bypass Ratio
NM	Nautical Mile	VAFN	Variable Area Fan Nozzle
NPSS	Numerical Propulsion System Software	VLM	Vortex-Lattice Method
OPR	Overall Pressure Ratio	WATE++	Weight Analysis of Turbine Engines

[1] Ph.D. Student, Department of Mechanical, Manufacturing and Biomedical Engineering.
[2] Assistant Professor, Department of Mechanical, Manufacturing and Biomedical Engineering.
[3] Professor, Department of Mechanical, Manufacturing and Biomedical Engineering.

II. Introduction

Aviation's CO_2 emissions could reach an annual output of two million tonnes by 2050, i.e. more than double the emissions in 2019, according to projections by the Air Transport Action Group (ATAG) using an annual traffic growth rate of 3.1% [1]. Therefore, achievable decarbonisation pathways must be identified to enable sustainable growth of the industry. One such pathway identified by ATAG is their 'aggressive technology' pathway, which projects 53% of the emission reductions being achieved through deployment of Sustainable Aviation Fuel (SAF), and 34% of emission reductions arising from aircraft technology improvements – which include disruptive technologies such as electrified and hydrogen powered aircraft, coupled with novel airframe and engine developments [1]. These efficiency improvements are of paramount importance in reducing the overall energy demand of aviation, and therefore also reducing the demand for scarce, expensive alternative fuels such as SAF. Furthermore, technologies that significantly enhance fuel efficiency have the potential to enable the transition to lower-performance, but highly-sustainable, carbon-free technologies, such as electric and hydrogen-powered aircraft – particularly for short-haul flights.

Generally, a major source of efficiency enhancements for next-generation aircraft are derived from the power-plant. For example, the current generation Boeing 737-8200 is claimed to reduce fuel consumption by greater than 16% compared to the B737-800NG [2]. The bulk of these fuel burn reductions are attributable to the transition from the CFM56-7B engine to the more efficient LEAP-1B turbofan, as the LEAP engine Thrust Specific Fuel Consumption (TSFC) was >20% lower at Sea-Level Static (SLS) conditions according to the International Civil Aviation Organisation (ICAO) emissions databank [3]. Given the increased urgency for emission reductions, disruptive engine technologies are being explored for next-generation aircraft. Within these advanced engine options are the Ultra-High Bypass Ratio (UHBPR) turbofan and the Contra-Rotating Open Rotor (CROR) engine, pictured in Fig. 1 (a) and (b), respectively.

The UHBPR turbofan may be described as an evolutionary design, or the natural progression from the high-bypass LEAP engine. This design extends the Bypass Ratio (BPR) of the turbofan to the limits of installed-turbofan performance (BPR ≈ 15-25), carefully considering the trade-offs between engine TSFC and the installed-engine performance, which accounts for the total effects of the system in terms of the increased nacelle weight and drag. Numerical studies show that the UHBPR turbofan could achieve TSFC values of 12.2-13.7 (g/kN·s) during cruise [4], [5], [6], [7], which represents a reduction of 21.8-30.6% compared to the TSFC of the CFM56-5B turbofan developed in 2000 [5].

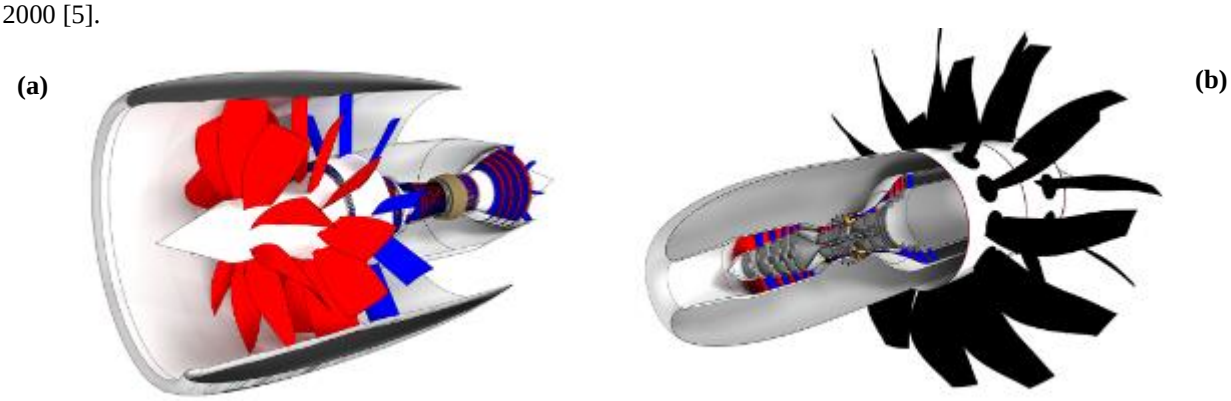

Fig. 1 Advanced propulsion systems for next-generation aircraft (a) UHBPR turbofan (b) CROR engine [6]

The CROR engine utilises a novel, external propeller design, similar to an advanced turboprop engine. The external propellers enable extremely large BPRs (potentially >70:1 [8]), which significantly improve the propulsive efficiency, and hence the TSFC. The propeller designs are shape-optimised to mitigate shockwaves at high speeds, utilise variable pitch functionality to maintain high performance over a wide range of operating conditions, and employ a set of counter-rotating or stator-blades to de-swirl the flow and maintain high propulsive efficiencies. Furthermore, the nacelle weight and drag is minimised by using an unshrouded design, alleviating a considerable portion of the performance penalties imposed on the installed engine performance in the case of the UHBPR turbofan. Numerical studies of the CROR prop-fan report cruise TSFCs between 10.4-12.1 (g/kN·s) [4], [6], [9], representing a TSFC reduction of 30.9-40.6% compared to the CFM56-5B turbofan.

While previous studies have predicted the TSFC performance of each advanced engine technology at design points such as Top-Of-Climb (TOC), Rolling Take-Off (RTO) and cruise [4], [5], [6], [7], [9], [10], [11], [12], [13], current

research lacks a thorough investigation into the installed engine performance over a complete flight operation schedule to assess the real-world benefits achievable with each technology. This is of particular importance for these two technologies due to their different performance characteristics – the UHBPR turbofan yields an optimum performance during its mid-cruise operating point, highlighted in Fig. 2 (a), whereas the CROR engine yields optimum performance close to its maximum power operating point, as illustrated in Fig. 2 (b). Furthermore, the enhanced BPRs of the CROR engine result in even greater propulsive efficiency improvements during low-speed segments, such as take-off and climb, compared to the UHBPR turbofan [4]. These distinctions in performance characteristics could mean that CROR engines exhibit even greater performance benefits over the UHBPR turbofan for highly-loaded, short-haul flights, which spend a significant portion of the flight time during high-powered operations, such as take-off and climb.

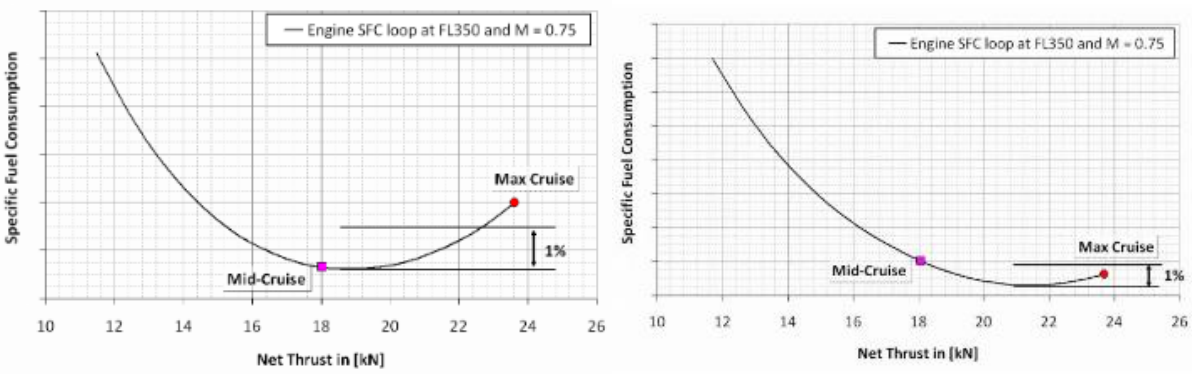

Fig. 2 TSFC as a function of net thrust for (a) UHBPR turbofan (b) CROR engine [9]

Therefore, the aim of this study is to evaluate the real-world performance benefits of an UHBPR turbofan and CROR engine for short-haul aircraft through simulation of each advanced aircraft configuration over a full, real-world operation schedule of Europe's largest airline. Baseline aircraft models of the Boeing 737-800NG (B737-NG) and Boeing 737-8200 (B737-MAX) aircraft were developed, validated, and calibrated over a wide-range of real-world flight data using a novel real-world operations model, following a similar method described in the author's previous work [14]. Advanced aircraft configurations with the UHBPR and CROR propulsion systems were subsequently developed and evaluated over a full day of the airline's operations to and from Irish airports, where the cumulative fuel burn performance for each configuration was quantified and compared against the baseline model. Specific objectives of this work included:

- Development of baseline propulsion system models of the CFM56 and LEAP turbofans
- Development of baseline aircraft models of the B737-NG and B737-MAX aircraft
- Development of a novel real-world operations model to accurately simulate real-world flights
- Validation/calibration of the baseline model performance against real-world flight data for 50 flights
- Development of advanced propulsion system models for the UHBPR turbofan and CROR engine
- Validation of the numerical model predictions against results from previous numerical studies
- Simulation of each aircraft over a full day of Irish operations (257 flights)
- Comparison of the real-world performance in terms of fuel burn, emissions, and cost

III. Baseline Aircraft Model

A. Model Components

1. Aerodynamic Model

A representative model of the B737-NG and B737-MAX aircraft were developed using the open-source Stanford University Aerospace Vehicle Environment (SUAVE) conceptual design tool [15], where details of the aircraft geometry were obtained from airport planning reference sheets [16]. SUAVE contains a suite of physics-based and semi-empirical methods for aerodynamics, propulsion, and mission analysis calculations [15]. The physics-based 'fidelity-zero' Vortex-Lattice Method (VLM), which was previously validated against experimental data [17], was used to model the inviscid lift and induced drag of the aircraft. Semi-empirical methods within SUAVE were used for the drag build-up based on correlations provided by Shevell [15], [18]. Correction factors within these semi-empirical methods were utilised for calibration of the aerodynamic model, as discussed in Section III D.

2. Propulsion System Model

A numerical model of the CFM56-7B26 and LEAP-1B27 turbofans were developed using the Numerical Propulsion System Simulation (NPSS) tool. NPSS was chosen as the propulsion system modelling tool for this study due to the extensive use of the software throughout published research [7], [10], [19], [20], along with documented validations [7], [14], [21], and builds upon expertise developed in previous work [14], [22]. A component diagram of the general NPSS turbofan model is illustrated in Fig. 3. The numerical model was calibrated through variation of the design variables for each component, such as the fan pressure ratio, burner temperature (T4), Bypass Ratio (BPR), inlet mass flow, desired blade/vane temperatures of the turbines, alongside constraints such as the maximum allowable burner temperature and shaft speeds. The BPR of the LEAP engine was set such that the jet velocity ratio at the design point, i.e. TOC, was equal to 1.6 [23]. Generalised component performance maps, developed by NASA as part of their energy efficient engine programme [24], were utilised to characterise the compressor and turbine off-design performance, whereas the NASA CoolIt subroutine was utilised to calculate turbine cooling requirements [25]

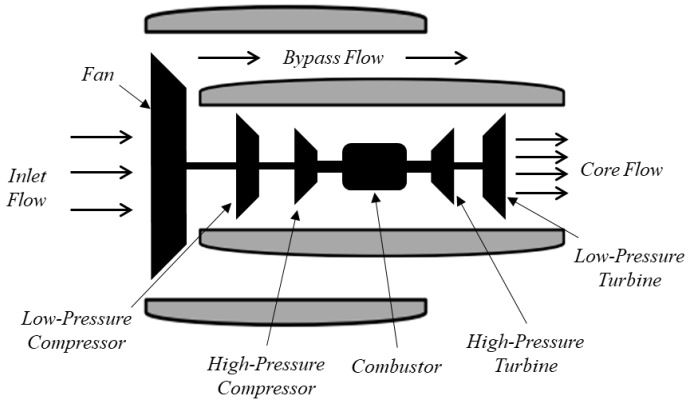

Fig. 3 Component diagram of CFM56-7B26 and LEAP-1B27 turbofan models developed using NPSS

The CFM56 and LEAP turbofan models were validated against publicly available data measured by the ICAO for four SLS operating points, ranging from 7% to 100% thrust values. Table 1 shows the validation results for the SLS operating points, alongside the performance of the engine at TOC and RTO. The thrust value shown for TOC is the engine's maximum thrust at 35,000 ft and a Mach number of 0.8, whereas the RTO and SLS-100 operating points show the maximum hot-day thrust (i.e. ISA+15°C) at Mach numbers of 0.25 and 0, respectively, both of which are at sea-level altitude. The validation results show that the NPSS models achieved a high-level of accuracy, as the thrust and TSFC of the two most critical SLS points (SLS-100 and SLS-85) were predicted with < 1% error magnitudes. The remaining SLS operating points (SLS-30 and SLS-07), which are less critical due to the lower fuel-flow rates and limited relevance to the in-flight performance, were predicted with an accuracy of 2.1% – 4.3% and 0.4% – 2.8%, respectively.

Table 1 Validation results for CFM56-7B26 and LEAP-1B27 turbofan models developed using NPSS

	CFM56-7B26/3			LEAP-1B27		
Op. Point	**Predicted TSFC** *(lbf/hr·lbm)*	**ICAO TSFC** *(lbf/hr·lbm)*	**TSFC Error**	**Predicted TSFC** *(lbf/hr·lbm)*	**ICAO TSFC** *(lbf/hr·lbm)*	**TSFC Error**
TOC	0.634	-	-	0.557	-	-
RTO (+15°C)	0.487	-	-	0.406	-	-
SLS – 100%	0.365	0.366	-0.34%	0.288	0.287	0.28%
SLS – 85%	0.351	0.350	0.36%	0.277	0.275	0.67%
SLS – 30%	0.319	0.333	-4.25%	0.252	0.258	-2.11%
SLS – 7%	0.479	0.466	2.77%	0.383	0.385	-0.44%

3. Propulsion Surrogate Model

In order to integrate the NPSS models with the total aircraft model, propulsion surrogate models were developed for the CFM56 and LEAP turbofan engines. To develop the surrogate models, discrete engine decks were generated by simulating the NPSS models at a full range of altitude, Mach numbers, and throttle values, recording the thrust and

TSFC for each operating point. The two surrogate models representing the thrust and the TSFC were generated using Gaussian regression methods [22].

B. Real-World Operations Model

The real-world operations model in this study represents a key novel aspect of this research. This work aims to enhance the coupling between aircraft conceptual design and flight operations, to predict the real-world benefits obtained with each technology, and identify the key technology drivers of decarbonisation for a given operational strategy. The real-world operations model was developed to generate flight paths for the SUAVE mission analysis module, based on the actual flight paths and TOWs of the airline's flights. This study uses a similar approach to the author's previous work [8], albeit with a significantly larger flight database, and improved flight data derived from on-board Quick-Access Recorder (QAR) data, compared to the publicly available Automatic Dependent Surveillance-Broadcast (ADS-B) data used in the previous study – which did not account for the true airspeed of each flight.

1. Real-World Flight Database

An extensive flight database was provided to the authors, consisting of QAR data for a full day of B737-NG operations (2457 flights), alongside a further 23 B737-MAX flights, with a data sample rate of 1 Hz and 9 Hz, respectively. The flight database provided a valuable opportunity to conduct a rigorous validation and calibration study to evaluate and maximise the accuracy of the selected conceptual design tool. The distribution of mission range and Take-Off Weight (TOW) within the flight database is illustrated in Fig. 4, where the TOW values are redacted due to the sensitive nature of the data, but the variation of TOW values is indicated on the graph. There was significant variation in the mission range, ranging from 88 NM to 2320 NM, with an average mission range of 693 NM, which is closely aligned to the airline's annual average mission range of 766 NM in 2023 [2].

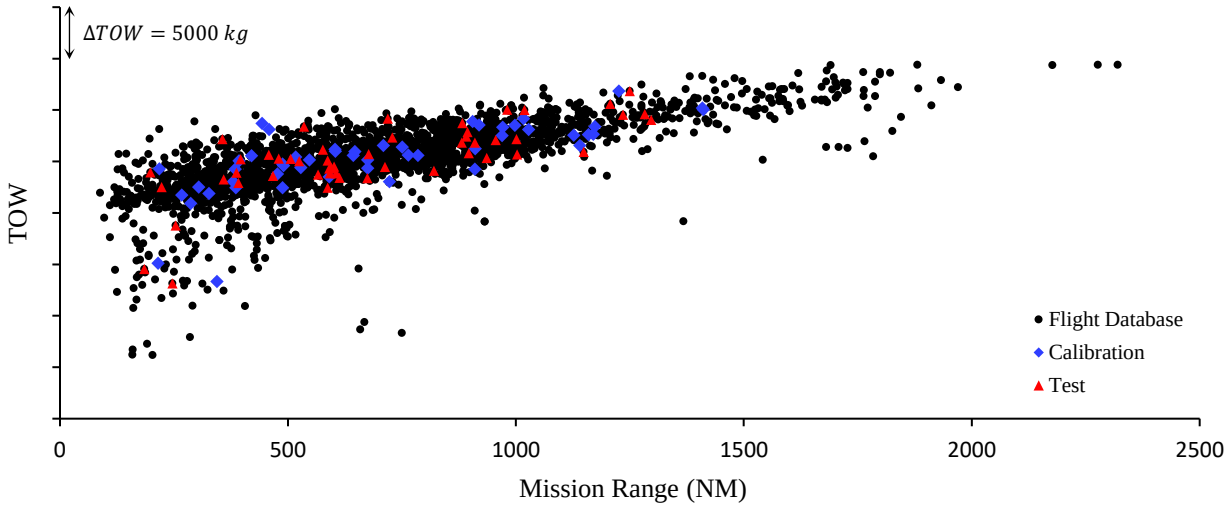

Fig. 4 Distribution of range and TOW of the B737-NG flight database and calibration/test datasets

To perform the calibration of the B737-NG aircraft model, a subset of 50 B737-NG flights were selected from the flight database and place into the calibration dataset. In order to maintain sufficient representation of the wider database, the calibration dataset was generated such that the mean of the mission range and TOW were kept within 1% of the complete flight database, while the sample standard deviations were maintained within 10% of the complete flight database. The 50 selected flights are illustrated in Fig. 4, superimposed on the complete flight database. Using the same approach, a further 50 flights were placed in the B737-NG test dataset. Due to the limited available data for the B737-MAX aircraft, 19 flights were manually selected and placed in the calibration dataset, leaving four remaining flights that were placed in the test dataset.

2. Flight Path Approximation

In order to simulate each of the real-world flights within SUAVE, the flight paths were approximated in terms of piece-wise linear sub-segments which were input into the SUAVE mission analysis module. The flight paths were approximated in terms of altitude, Mach number, and Ground Speed (GS) with respect to the flight time, where 16

sub-segments were used for the climb and descent phases, and a variable number of cruise and step-climb segments were used to accurately capture the cruise profile.

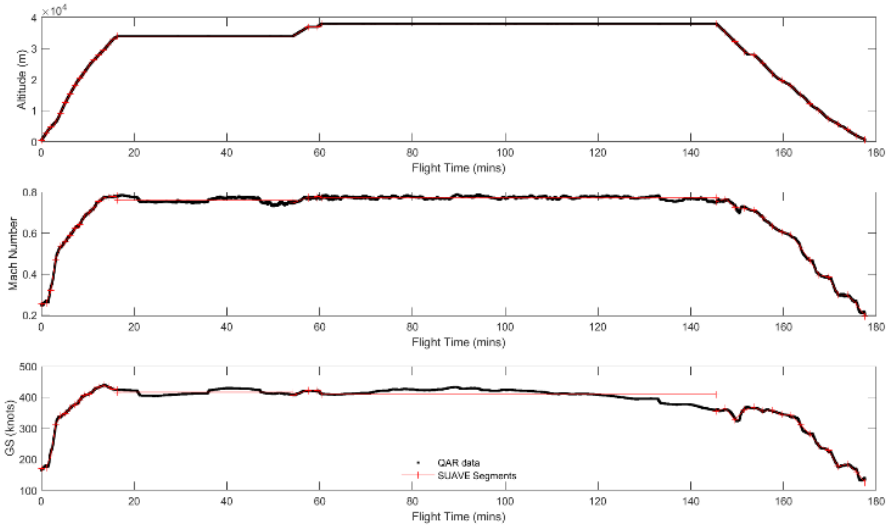

Fig. 5 Flight path approximation in terms of altitude, Mach number and ground speed for multi-cruise B737-NG flight

Fig. 5 shows an example flight path approximation of a multi-cruise flight with step-climb segments. The linear SUAVE flight paths were approximated using a least-squares approach in an automated MATLAB software routine, formulated using the QAR flight data. The generated SUAVE segments are highlighted in Fig. 5, which show good agreement with the actual flight paths obtained from the QAR data. The flight segments within the climb and descent phases were simulated using a linear-Mach number and constant rate of climb/descent, whereas the cruise segments were simulated using a constant Mach number and constant altitude. During the flight simulations, the linearised equations of motion were solved to achieve convergence for each segment within the mission. More details on the SUAVE mission simulation process can be obtained from Lukaczyk et al. [15].

C. Baseline Aircraft Validation

The aerodynamic model, propulsor surrogate models, and real-world operations model were combined to generate the total baseline aircraft model. A preliminary validation of the B737-NG and B737-MAX baseline aircraft models was performed using the standard, un-calibrated aerodynamic model, against the testing datasets described in Section III B2. The total average fuel-flow and fuel burn error magnitudes for the calibration and test datasets are outlined in Table 2.

Table 2 Preliminary validation of test flight datasets for B737-NG and B737-MAX models

Segment	Initial Climb	Climb	Cruise	Descent	Final Approach	Climb&Cruise	Total Fuel Burn
B737-NG-Cal.	3.7%	2.4%	4.0%	16.3%	50.4%	3.2%	2.2%
B737-NG-Test	3.5%	2.6%	4.0%	14.3%	50.2%	3.3%	2.2%
B737-MAX-Cal.	7.0%	4.0%	8.4%	13.5%	55.0%	6.2%	4.1%
B737-MAX-Test	8.8%	5.0%	9.5%	15.9%	57.2%	7.2%	4.9%

D. Baseline Aircraft Calibration

The aerodynamic coefficients associated with the semi-empirical methods used for the drag build-up were optimised in order to minimise the average predicted fuel-flow errors against the real-world flight data, following a similar method used in the author's previous work [14]. The aerodynamic model calibration utilised the B737-NG data due to the limited available data for the B737-MAX aircraft, where the average climb and cruise fuel-flow error magnitudes were minimised using the Sequential Least-Squares Quadratic Programming (SLSQP) minimisation algorithm in the SciPy Python library.

The calibration variables, along with the initial values the calibration range, and the optimised values are presented in Table 3. Furthermore, the drag polars were modified for the take-off and landing segments to account for the flaps, slats, and landing gear. The drag polars for these configurations were modified through optimisation of a drag

coefficient increment to minimise the average fuel-flow errors of the first and last flight segments, using the same optimisation methods outlined above. The calibration parameters for this optimisation are also listed in Table 3. Finally, the descent segment was calibrated by imposing a minimum idle throttle condition, in which a drag coefficient increment was calculated and added to the aircraft model such that the lowest thrust value was equal to the minimum idle thrust for the given altitude and Mach number.

While the B737-NG and B737-MAX share an almost identical airframe, the B737-MAX was designed with a number of minor aerodynamic improvements, such as the addition of split wing-tips and the removal of the aft body vortex generators [27] – features which the low-fidelity aerodynamic model cannot capture. Because of this, a Lift/Drag (L/D) increment was calibrated and implemented to the B737-MAX model, resulting in a 3.56% increase in the L/D performance across the entire drag polar, as outlined in Table 3.

Table 3 Calibration variables used to optimise the VLM aerodynamic model

Aircraft Calibration	Calibration Variable	Initial Value	Calibration Range	Optimised Value
B737-NG	Fuselage Lift	1.14	1.10 – 1.30	1.2668
	Trim Drag	1.02	1.01 – 1.05	1.0465
	Wing Drag	1.10	1.05 – 1.40	1.3374
	Fuselage Drag	2.30	2.00 – 3.00	2.1220
	Viscous Lift-Dependent Drag	0.38	0.30 – 0.50	0.4605
	Idle Thrust (%)	0.00	1.00 – 5.00	1.0000
	$C_{D,Take\text{-}off}$	0.00	0.00 – 0.03	0.0068
	$C_{D,Landing}$	0.00	0.00 – 0.10	0.0663
B737-MAX	*L/D* increment (%)	0.00	0.00 – 5.00	5.7400

Similarly to the previous section, all the flights from the testing datasets were simulated, with the introduction of the optimised calibration variables. Two flights are presented in Fig. 6, where the fuel-flow accuracy can be observed for each phase of flight. The total average fuel-flow and fuel burn error magnitudes for the complete calibration and test datasets are outlined in Table 4, which highlight the model improvements, and the exceptional accuracy of the low-fidelity model with respect to real-world flight data for a wide range of flights.

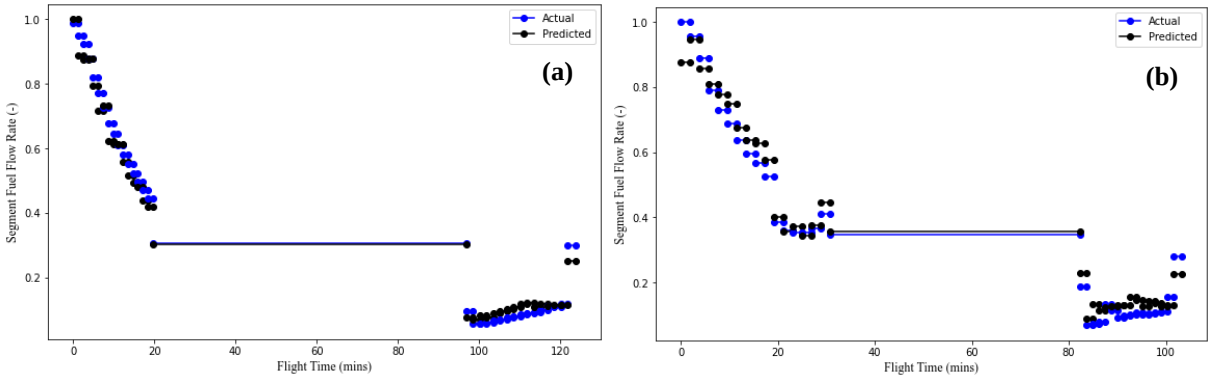

Fig. 6 Fuel-flow validation for the calibrated SUAVE-NPSS model (a) B737-NG (b) B737-MAX

Table 4 Final validation of test dataset for calibrated B737-NG and B737-MAX models

Segment	Initial Climb	Climb	Cruise	Descent	Final Approach	Climb&Cruise	Total Fuel Burn
B737-NG-Cal.	3.5%	2.9%	1.8%	6.6%	8.0%	2.4%	1.4%
B737-NG-Test	3.2%	3.1%	1.9%	5.7%	8.8%	2.5%	1.6%
B737-MAX-Cal.	5.7%	1.9%	1.4%	6.6%	7.4%	1.7%	1.6%
B737-MAX-Test	7.5%	1.1%	0.9%	7.4%	7.1%	1.0%	1.6%

IV. Advanced Aircraft Model

E. UHBPR Turbofan

A numerical model of the UHBPR turbofan was subsequently developed, using the generalised NPSS turbofan model outlined in Section III A1, where the design variables were selected to match those outlined in the NASA N+3 study described by Jones et al. [7]. The significant changes with respect to the baseline turbofan models lie in the increased BPR and OPR, which were increased to 24 and 55, respectively. Furthermore, the UHBPR model utilised increased allowable combustor temperatures (T4 = 3400°R) alongside ceramic matrix composite materials to reduce turbine cooling requirements, and a gearbox to enable optimum fan and low-pressure compressor rotational speeds. A Variable Area Fan Nozzle (VAFN) was also included to maintain fan operation on the peak efficiency operating line throughout the flight envelope, which was done through assignment of the bypass nozzle area as an independent variable to target the peak efficiency R-line for each corrected speed within the fan map data.

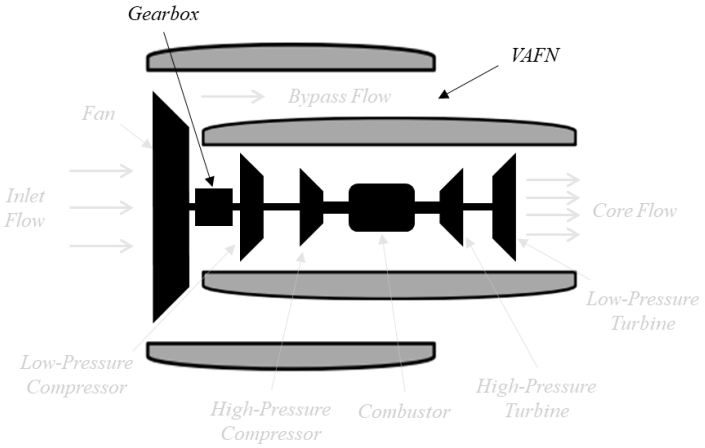

Fig. 7 Component diagram for UHBPR turbofan model with additional model components highlighted

The UHBPR turbofan model performance was validated against the N+3 model developed by Jones et al. [7], for the TOC, RTO, Cruise (CRZ) and SLS operating conditions. Table 5 shows good agreement between the predicted thrust and TSFC of the developed model when compared to the N+3 NASA numerical model, providing confidence in the validity and accuracy of the numerical model performance predictions.

Table 5 Validation results for UHBPR turbofan model against NASA N+3 numerical model [7]

	UHBPR Turbofan Model		**NASA N+3 Turbofan** [7]		
Op. Point	**Predicted Thrust** *(lbf)*	**Predicted TSFC** *(lbf/hr·lbm)*	**Predicted Thrust** *(lbf)*	**Predicted TSFC** *(lbf/hr·lbm)*	**ΔTSFC**
TOC	6082	0.460	6073	0.464	-0.86%
CRZ	5473	0.462	5466	0.464	-0.43%
RTO (+15°C)	22731	0.288	22800	0.289	-0.03%
SLS (+15°C)	28656	0.175	28621	0.175	0.00%

F. CROR Engine

3. Model Setup

A numerical model of the Contra-Rotating Open-Rotor (CROR) engine, based on the GE36 Un-Ducted Fan (UDF) design proposed in the 1980s, was developed using NPSS following the methods outlined by Hendricks and Tong [12]. The CROR engine consists of a turbojet core, followed by a free-power turbine coupled to a set of counter-rotating propeller blades through a gearbox at the rear side of the engine. The design parameters within the core of the CROR engine were chosen to match those used for the UHBPR turbofan in order to maintain a consistent analysis between the two propulsion systems, whereas the CROR core mass flow was scaled such that the thrust output at TOC and RTO matched that of the UHBPR turbofan. The component diagram representing the developed NPSS model is illustrated in Fig. 8.

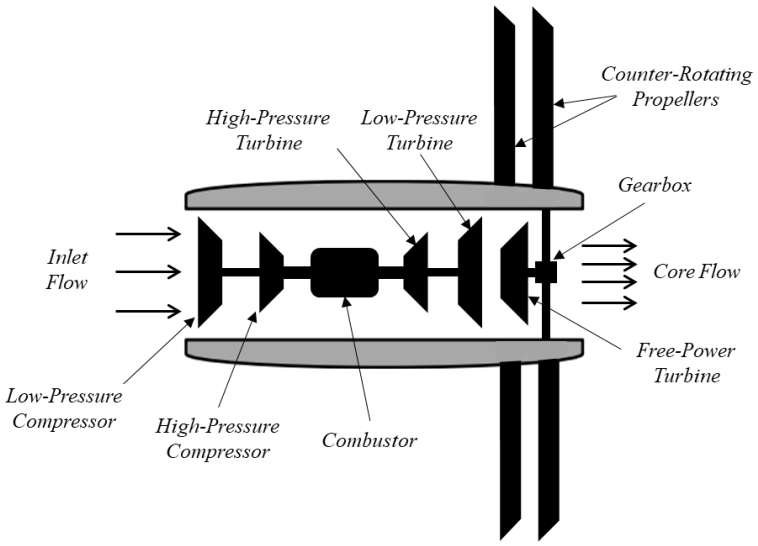

Fig. 8 Component block diagram for proposed OR engine models (a) CROR (b) RISE open-fan

4. Propeller Maps

The representation of the counter-rotating propeller performance represents a challenge in the development of numerical models for the CROR engine due to the lack of comprehensive performance maps [11], [28], [29]. Initially, map data for the F7/A7 propellers obtained from a NASA study in the 1990s was transcribed and developed into NPSS performance maps, however it was found that the data was excessively sparse to characterise the performance across the entire flight envelope, leading to inaccurate performance predictions at off-design conditions. Following this, the multivariate regression equations developed by Hendricks [28] were used to estimate the thrust and power coefficients, however, the accuracy of this method also proved to be insufficient to accurately characterise the off-design performance. Instead, the scaled F7/A7 propeller performance maps developed by Perullo et al. [11] were transcribed and developed into an NPSS performance map, to be used in conjunction with a modified NPSS propeller element. The maps developed by Perullo et al. [11] were created by scaling a standard propeller performance map until the performance matched those obtained from the original F7/A7 counter-rotating propeller maps, and were used for the current study due to the completeness of the data across a wide range of advance ratios and blade angles, which enabled simulations spanning the entire flight envelope. Note that the SLS operating points were not simulated for the CROR engine due to the lack of propeller map data for advance ratios between 0 – 0.5. However, these points were not required for the flight operations simulated in Section V.

5. Power Management Strategy

The CROR engine was operated using a constant tip speed strategy, as employed by Hendricks and Tong [12] and Perullo et al. [11], where the current study employed the propeller blade angle as an independent variable within NPSS to target a propeller tip speed of 785 ft/s. This resulted in a decreasing blade pitch angle with decreasing Mach number and decreasing throttle, where the blade pitch angle decreased from 60 to 53.6 degrees at TOC, and from 40.3 to 26.7 degrees at RTO. Similar results for this power management strategy were also reported by Hendricks and Tong [12].

6. Validation

The CROR NPSS model validated against the numerical model developed by Hendricks and Tong [12] through comparison of the TSFC characteristics for different throttle settings at the TOC and RTO flight conditions, where the design variables of the core were modified to match those used in the Hendricks model. Fig. 9 shows the TSFC performance predictions for the current CROR model and the Hendricks CROR model, where good alignment is observed for both TSFC curves. The most significant differences in the predicted TSFC occur at the mid-power point for RTO, and the low-power operations for both TOC and RTO, which are likely due to the different sources used for the propeller map data. However, the difference in performance predictions is minimal for the vast majority of throttle settings, and therefore this validation provides confidence in the performance predictions of the developed NPSS CROR model, and hence the propeller maps used to represent the contra-rotating propeller performance.

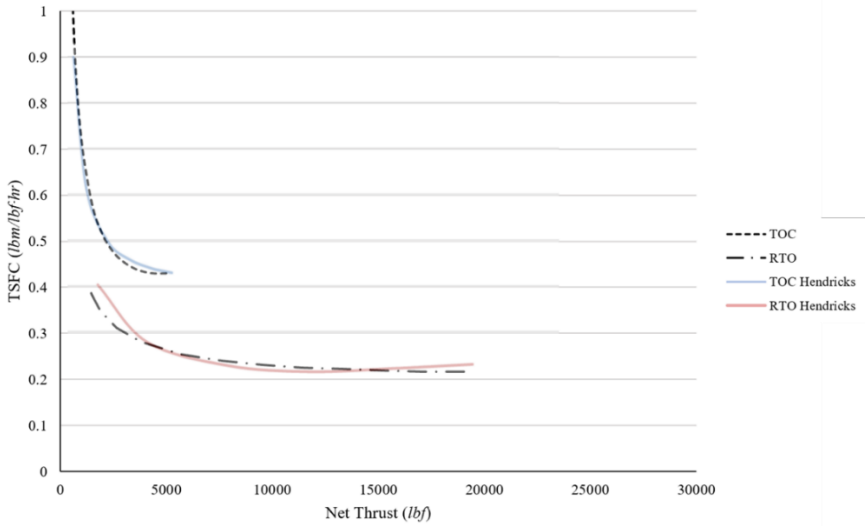

Fig. 9 Validation of CROR model TSFC curves against Hendricks model [12]

G. Advanced Aircraft Configurations

Advanced aircraft configurations were developed by combining the advanced propulsion systems, i.e. the UHBPR turbofan and the CROR engine, with the B737-MAX airframe. Similarly to the baseline aircraft model, surrogate propulsion system models were developed for the UHBPR and CROR engines using Gaussian methods [30], which were integrated into each SUAVE aircraft model.

Due to the increased mass of the advanced propulsion systems compared to the LEAP engine, the Operating Empty Weight (OEW) and nacelle geometry of each advanced aircraft configuration had to be modified. The UHBPR turbofan was predicted to have a total system mass of 9300 lbs., representing a 1600 lbs. (+21%) increase over the CFM56 engine following a WATE++ (Weight Analysis of Turbine Engines [31]) analysis performed by Jones et al. [7], whereas the LEAP engine is reported to have a 16% greater mass than the CFM56 engine. The total system mass of the LEAP turbofan is unknown, therefore it was assumed that the total system mass of the LEAP engine was 16% greater than the CFM56 at 8932 lbs. The CROR engine developed by Hendricks and Tong [12] was predicted to have a total system mass of 9220 lbs. using WATE++, with the core section accounting for 4950 lbs. As the core mass flow of the CROR engine used in the current study was increased by 29% to match the thrust ratings of the UHBPR turbofan, the mass of the core was scaled by the same factor, resulting in a core mass of 6392.7 lbs. and a total system mass of 10662.7 lbs. The difference in the total propulsion system mass for each engine compared to the LEAP engine was added to the OEW of each advanced aircraft configuration. The final aircraft parameters for each aircraft configuration to be evaluated over the operation schedule are outlined in Table 6.

Table 6 Aircraft parameters for baseline and advanced aircraft configurations

Configuration	B737-MAX-Baseline	B737-MAX-UHBPR	B737-MAX-CROR
MTOW (*kg*)	82644	82811	83430
OEW (*kg*)	44130	44297	44916
Propulsion System Mass (*kg*)	4051	4218	4837
Fan/Propeller Diameter (*m*)	1.75	2.54	4.21
Fan/Propeller Efficiency (*%*)	91	96.9	85.0
BPR	8.0	24.0	-
OPR	41.5	55.0	42.0
TOC Thrust (*lbf*)	5974	6082	6074
RTO Thrust (*lbf*)	22798	22731	22842
SLS Thrust (*lbf*)	28144	28656	-
TOC TSFC (*lbf/hr·lbm*)	0.557	0.460	0.420
CRZ TSFC (*lbf/hr·lbm*)	0.547	0.462	0.415
RTO TSFC (*lbf/hr·lbm*)	0.406	0.288	0.206
SLS TSFC (*lbf/hr·lbm*)	0.288	0.175	-

V. Advanced Propulsion System Evaluation

H. Operation Schedule

The operation schedule selected for the case study consisted of the flights to and from any Irish airports, i.e. Dublin, Belfast, Cork, Shannon and Knock, within the full day of B737-NG operations. The final schedule consisted of 257 B738-NG flights, and the average mission range of these 257 flights was 659 NM. The flight paths for each mission were developed using the real-world operations model outlined in Section III B, whereas the TOW values for each flight simulation were calculated by adding the difference in OEW values between the B737-NG aircraft and the B737-MAX configurations listed in Table 6 to the TOW values contained within the flight database, which was described in Section III B1.

I. Performance Benefits

The performance benefits obtained for the UHBPR and CROR configurations when compared to the LEAP-powered B737-MAX configuration are presented in Fig. 10. Overall, both configurations exhibited a significant performance improvement over the baseline configuration. The UHBPR configuration yielded performance benefits ranging from 12.5% - 17.4% with an average value of 14.5%, compared to 20.6% - 29.0% for the CROR engine, which yielded an average performance benefit of 23.9% compared to the baseline aircraft.

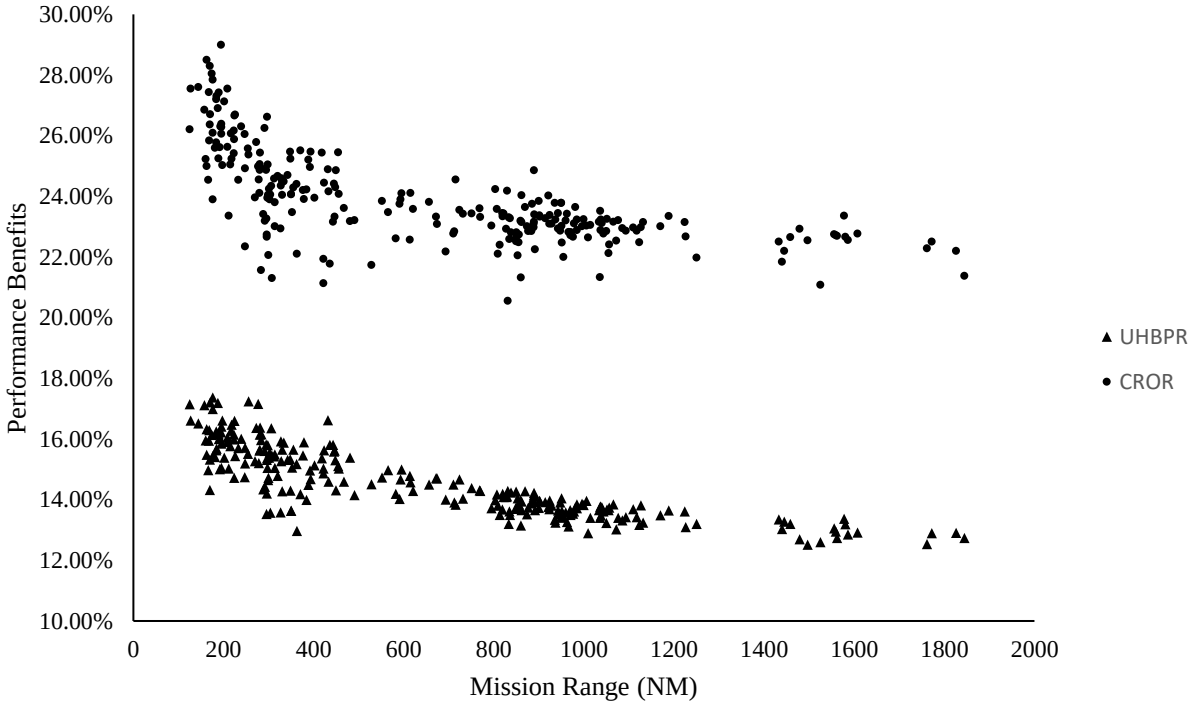

Fig. 10 Performance benefits for UHBPR and CROR configurations against the B737-MAX baseline model

Clearly, the CROR represents a step-change in performance across the full range of missions analysed, however, a more interesting observation is found in the trend in performance benefits for short-range missions. It was hypothesised in Section I that the CROR engine would result in greater benefits for a short-haul airline with a low average mission range and high load-factors due to the increased performance at high-power and low-speed, which is observed in the results displayed in Fig. 10. While such observations may seem trivial, these studies are important to quantify the benefits available to airlines to encourage investment in fleet renewals for more sustainable aircraft. Furthermore, such studies can be integrated into larger fleet-optimisation studies, in which flight schedules are optimised to extract the most benefits out of advanced aircraft configurations, and further reduce the energy demand, and hence the emissions, of the aviation industry.

J. Fleet-Wide Performance

The fleet-wide performance of the baseline and each advanced aircraft configuration is outlined in Table 7. The UHBPR and CROR configurations resulted in a total fuel burn reduction of 130.2 tonnes and 216.7 tonnes, respectively, whereas the total CO_2 emission reductions were 2.52 million tonnes and 2.25 million tonnes for the UHBPR and CROR engine, respectively. This resulted in a total fuel and emission reduction of 14.0% and 23.3% for the operation schedule, which is marginally lower than the average performance benefits for each flight outlined in the previous section due to the increased benefits for short-range missions. It must be noted that the results shown here only account for approximately 10% of the airline's daily flights, and therefore the fuel burn and emission reductions would likely be an order of magnitude higher for a full day of operations. These results highlight the significant impact that advanced propulsion systems can have on short-haul operations in terms of both emissions and fuel cost, which should encourage investment into fleet renewal for more sustainable aircraft operations.

Table 7 Fleet-wide performance in terms of fuel burn and emissions for the simulated operation schedule

	B737-MAX-Baseline	B737-MAX-UHBPR	B737-MAX-CROR
Total Fuel Burn (kg)	928,727	798,512	712,056
Δ Fuel Burn (kg)	-	-130,215	-216,671
Total CO_2 (Mt)	2.935	2.523	2.250
Δ CO_2 (Mt)	-	0.412	0.685
Total Reductions	-	14.0%	23.3%

VI. Conclusions

A validated and calibrated physics-based model was adapted to evaluate the real-world performance benefits that can be expected for the UHBPR turbofan and CROR engine across a representative flight operation schedule using a novel real-world operations model. The baseline model was validated over a wide range of real-world flight data, resulting in average total fuel burn errors between 1-1.5% for the B737-NG and B737-MAX, respectively. The B737-MAX baseline model was subsequently adapted to incorporate the advanced propulsion system models, which were developed using NPSS and validated against similar numerical studies. Each advanced aircraft was simulated over a full day of airline flights to and from Irish airports, where the performance of each configuration was compared to the baseline B737-MAX in terms of fuel and CO_2 emissions. As expected, the CROR exhibited a step-change in performance benefits against the baseline aircraft, with an average fuel burn reduction of 23.9%, compared to 14.5% for the UHBPR turbofan. Interesting trends were observed in the performance of the CROR engine, which yielded significantly increased performance benefits for mission ranges below 500 NM, due to the increased performance during climb and take-off segments. This study serves as a realistic gauge into the expected performance benefits for next-generation aircraft, while identifying the optimum missions that airlines should utilise when integrating advanced aircraft into the fleet. Future studies will be expanded into full fleet-optimisation studies, where advanced aircraft are allocated to the optimum routes across a full operation schedule. These studies aim to encourage investment into fleet renewal and sustainable aircraft by evaluating the business case for next-generation aircraft to promote an environmentally and economically sustainable transition to net-zero flights in 2050.

Acknowledgements

The authors would like to thank Ryanair for the financial and technical support of this study through the Sustainable Aviation Research Centre at Trinity College Dublin, along with the permission to use their data.

References

[1] "Waypoint 2050." Accessed: Jul. 05, 2022. [Online]. Available: https://aviationbenefits.org/environmental-efficiency/climate-action/waypoint-2050/

[2] "Ryanair | Results Centre." Accessed: Sep. 22, 2022. [Online]. Available: https://investor.ryanair.com/results-centre/

[3] "ICAO Aircraft Engine Emissions Databank," EASA. Accessed: Oct. 20, 2022. [Online]. Available: https://www.easa.europa.eu/en/domains/environment/icao-aircraft-engine-emissions-databank

[4] F. S. Mastropierro, J. Sebastiampillai, F. Jacob, and A. Rolt, "Modeling Geared Turbofan and Open Rotor Engine Performance for Year-2050 Long-Range and Short-Range Aircraft," *Journal of Engineering for Gas Turbines and Power*, vol. 142, no. 4, Feb. 2020, doi: 10.1115/1.4045077.

[5] D. Mo, I. Roumeliotis, C. Mourouzidis, S. Kissoon, and Y. Liu, "Assessment of Performance Boundaries and Operability of Low Specific Thrust GUHBPR Engines for EIS2025," *Journal of Engineering for Gas Turbines and Power*, vol. 144, no. 7, May 2022, doi: 10.1115/1.4054405.

[6] S. Reitenbach *et al.*, "Design and Application of a Multidisciplinary Predesign Process for Novel Engine Concepts," *Journal of Engineering for Gas Turbines and Power*, vol. 141, no. 1, Sep. 2018, doi: 10.1115/1.4040750.
[7] S. M. Jones, W. J. Haller, and M. T.-H. Tong, "An N+3 Technology Level Reference Propulsion System," E-19373, May 2017. Accessed: Aug. 09, 2022. [Online]. Available: https://ntrs.nasa.gov/citations/20170005426
[8] "The Future Of Flight: Engine-Maker Unveils New Technology Development Program To Cut CO2 Emissions By 20% | GE News." Accessed: Dec. 12, 2023. [Online]. Available: https://www.ge.com/news/reports/the-future-of-flight-engine-maker-unveils-new-technology-development-program-to-cut-co2
[9] L. Larsson, T. Gro¨nstedt, and K. G. Kyprianidis, "Conceptual Design and Mission Analysis for a Geared Turbofan and an Open Rotor Configuration," presented at the ASME 2011 Turbo Expo: Turbine Technical Conference and Exposition, American Society of Mechanical Engineers Digital Collection, May 2012, pp. 359–370. doi: 10.1115/GT2011-46451.
[10] R. A. Clark, C. Perron, J. Tai, B. Airdo, and D. N. Mavris, "Development of an Open Rotor Propulsion System Model and Power Management Strategy".
[11] C. A. Perullo, J. C. M. Tai, and D. N. Mavris, "Effects of Advanced Engine Technology on Open Rotor Cycle Selection and Performance," presented at the ASME Turbo Expo 2012: Turbine Technical Conference and Exposition, American Society of Mechanical Engineers Digital Collection, Jul. 2013, pp. 259–269. doi: 10.1115/GT2012-69331.
[12] E. S. Hendricks and M. T. Tong, "Performance and Weight Estimates for an Advanced Open Rotor Engine," AIAA Paper 2012-3911, Sep. 2012. Accessed: Feb. 18, 2022. [Online]. Available: https://ntrs.nasa.gov/citations/20120014381
[13] C. Salpingidou, D. Misirlis, Z. Vlahostergios, M. Flouros, F. Donus, and K. Yakinthos, "Conceptual design study of a geared turbofan and an open rotor aero engine with intercooled recuperated core," *Proceedings of the Institution of Mechanical Engineers, Part G: Journal of Aerospace Engineering*, vol. 232, no. 14, pp. 2713–2720, Nov. 2018, doi: 10.1177/0954410018770883.
[14] C. Gallagher, C. Stuart, and S. Spence, "Validation and Calibration of Conceptual Design Tool SUAVE," in *AIAA AVIATION 2023 Forum*, in AIAA AVIATION Forum. , American Institute of Aeronautics and Astronautics, 2023. doi: 10.2514/6.2023-3225.
[15] T. W. Lukaczyk *et al.*, "SUAVE: An Open-Source Environment for Multi-Fidelity Conceptual Vehicle Design," in *16th AIAA/ISSMO Multidisciplinary Analysis and Optimization Conference*, Dallas, TX: American Institute of Aeronautics and Astronautics, Jun. 2015. doi: 10.2514/6.2015-3087.
[16] "Airport Compatibility - Airplane Characteristics for Aiport Planning." Accessed: Apr. 29, 2023. [Online]. Available: https://www.boeing.com/commercial/airports/plan_manuals.page
[17] E. M. Botero, M. A. Clarke, R. M. Erhard, J. T. Smart, J. J. Alonso, and A. Blaufox, "Aerodynamic Verification and Validation of SUAVE," in *AIAA SCITECH 2022 Forum*, in AIAA SciTech Forum. , American Institute of Aeronautics and Astronautics, 2021. doi: 10.2514/6.2022-1929.
[18] R. S. Shevell, *Fundamentals of Flight*. Prentice-Hall, 1983.
[19] J. Csank and G. L. Thomas, "Dynamic Analysis for a Geared Turbofan Engine with Variable Area Fan Nozzle," 2017. doi: 10.2514/6.2017-4819.
[20] G. L. Thomas, D. E. Culley, J. L. Kratz, and K. L. Fisher, "Dynamic Analysis of the hFan, a Parallel Hybrid Electric Turbofan Engine," in *2018 Joint Propulsion Conference*, Cincinnati, Ohio: American Institute of Aeronautics and Astronautics, Jul. 2018. doi: 10.2514/6.2018-4797.
[21] R. P. Thacker and N. Blaesser, "Modeling of a Modern Aircraft Through Calibration Techniques," in *AIAA Aviation 2019 Forum*, in AIAA AVIATION Forum. , American Institute of Aeronautics and Astronautics, 2019. doi: 10.2514/6.2019-2984.
[22] C. Gallagher, C. Stuart, and S. Spence, "Energy Analysis of Fleet Operations Using Green Liquid Hydrogen and Synthetic Kerosene," in *AIAA AVIATION 2023 Forum*, in AIAA AVIATION Forum. , American Institute of Aeronautics and Astronautics, 2023. doi: 10.2514/6.2023-4301.
[23] M. Guynn, J. Berton, K. Fisher, W. Haller, M. Tong, and D. Thurman, *Refined Exploration of Turbofan Design Options for an Advanced Single-Aisle Transport Aircraft*. 2011. doi: 10.13140/RG.2.1.2488.0726.
[24] P. G. Batterton, "Energy efficient engine program contributions to aircraft fuel conservation," presented at the Aviation Fuel Conservation Symp., Washington, DC, Jan. 1984. Accessed: Apr. 29, 2023. [Online]. Available: https://ntrs.nasa.gov/citations/19840021807
[25] J. W. Gauntner, "Algorithm for calculating turbine cooling flow and the resulting decrease in turbine efficiency," NASA-TM-81453, Feb. 1980. Accessed: Aug. 25, 2022. [Online]. Available: https://ntrs.nasa.gov/citations/19800011581
[26] "Ryanair traffic hits new record in August, up 12% year on year," *Reuters*, Sep. 04, 2023. Accessed: Dec. 07, 2023. [Online]. Available: https://www.reuters.com/business/aerospace-defense/ryanair-traffic-hits-new-record-august-up-12-year-year-2023-09-04/
[27] C. Brady, *The Boeing 737 Technical Guide*. Blurb, Incorporated, 2021.
[28] E. Hendricks, "Development of an Open Rotor Cycle Model in NPSS Using a Multi-Design Point Approach," 2011. doi: 10.1115/GT2011-46694.
[29] P. Bellocq, V. Sethi, L. Cerasi, S. Ahlefelder, R. Singh, and N. Tantot, "Advanced Open Rotor Performance Modelling for Multidisciplinary Optimization Assessments," presented at the ASME Turbo Expo 2010: Power for Land, Sea, and Air, American Society of Mechanical Engineers Digital Collection, Dec. 2010, pp. 287–302. doi: 10.1115/GT2010-22963.
[30] C. E. Rasmussen and C. K. I. Williams, *Gaussian processes for machine learning*. in Adaptive computation and machine learning. Cambridge, Mass: MIT Press, 2006.
[31] M. T. Tong and B. A. Naylor, "An Object-Oriented Computer Code for Aircraft Engine Weight Estimation," in *Volume 1: Aircraft Engine; Ceramics; Coal, Biomass and Alternative Fuels; Manufacturing, Materials and Metallurgy; Microturbines and Small Turbomachinery*, Berlin, Germany: ASMEDC, Jan. 2008, pp. 1–7. doi: 10.1115/GT2008-50062.